RSC Advances

This is an *Accepted Manuscript*, which has been through the Royal Society of Chemistry peer review process and has been accepted for publication.

Accepted Manuscripts are published online shortly after acceptance, before technical editing, formatting and proof reading. Using this free service, authors can make their results available to the community, in citable form, before we publish the edited article. This *Accepted Manuscript* will be replaced by the edited, formatted and paginated article as soon as this is available.

You can find more information about *Accepted Manuscripts* in the **Information for Authors**.

ROYAL SOCIETY
OF CHEMISTRY

www.rsc.org/advances

Differential Structural dynamics and antigenicity of two similar influenza H5N1 virus HA-specific HLA-A*0201-restricted CLT epitopes

Yeping Sun[1#], Qian Liu[2]

1. CAS Key Laboratory of Pathogenic Microbiology and Immunology, Institute of Microbiology, Chinese Academy of Sciences, Beijing 100101, P. R. China

2. Supercomputing Center, Chinese Academy of Sciences, Beijing 100101, P. R. China

Address correspondence to Yeping Sun, sunyeping@sun.im.ac.cn

Table of contents entry

The free RI-10 and KI-10 peptides showed bent rather than extended conformations as binding in the cleft of the HLA-A*0201 molecule, and KI-10-HLA-A*0201 processed a much higher flexibility than RI-10-HLA-A*0201.

Abstract: The presentation of viral peptides by major histocompatibility complex (MHC) molecules for T cell receptor (TCR) recognition is the central event in the development of T cell immunity against viruses. Molecular dynamics (MD) simulation is a powerful tool that is able to provide dynamic information, rather than a static view, of the mechanisms of peptide presentation in the antigen binding grooves of MHCs. In this paper, MD simulations are presented of two influenza H5N1 virus HA-specific cytotoxic T lymphocyte (CTL) epitopes, RI-10 (RLYQNPTTYI) and KI-10 (KLYQNPTTYI), in complex with HLA-A*0201. Although the amino acid sequence difference between RI-10 and KI-10 is slight, the structural dynamics of the two peptides were found to differ substantially. Molecular Mechanics/Poisson-Boltzmann Surface Area (MM/PBSA) calculations, and the thermal stability of the two complexes determined from their circular dichroism (CD) spectra, suggested that RI-10 had a higher binding free energy to HLA-A*0201 than KI-10. Furthermore, the structural fluctuation of the RI-10-HLA-A*0201 complex

was found to be significantly lower than that of KI-10-HLA-A*0201. The distinctive salt bridges formed between Arg1 of RI-10 with Glu63 of HLA-A*0201 and stronger hydrogen bond networks may contributed to different structural dynamics between the two pMHC complexes through dynamic allosteric interaction mechanisms. RI-10-containing H5N1 virus strains isolated from Chinese patients are much less prevalent than KI-10-containing strains; this correlates with the higher antigenic potency of RI-10 in comparison to KI-10, as demonstrated in HLA-A*0201/K[b] transgenic mice immunized with the two peptides.

Introduction

Major histocompatibility complex (MHC) class I molecules play a crucial role in initiating potentially protective immune responses by presenting intracellular pathogen-derived peptides to CD8^{+} cytotoxic T lymphocytes (CTLs), and thereby targeting infected cells for elimination. In the endoplasmic reticulum, the newly developed MHC class I molecules first select and bind potential CTL epitopes from a repertoire of peptides generated by the proteasome that is degrading the pathogen proteins; they then transport these epitopes to the cellular surface for T cell receptor (TCR) recognition [1].

The advent of structural data on peptide-MHC (pMHC) complexes led to a clearer understanding of the mechanisms of T-cell immune recognition. In 1987, Bjorkman et al. reported the first crystal structures of a pMHC, human leukocyte antigen (HLA)-A2, which revealed that the 3D structure of the cell-surface-expressed HLA class I molecule consisted of a highly variable heavy chain, comprising three alpha domains, in complex with a soluble invariant molecule, β2 microglobulin (β2M). The alpha 1 and alpha 2 domains of the heavy chain combine to make a four-stranded β sheet lined by two antiparallel helices, which together form a deep groove that binds the peptide [2-4]. More pMHC crystal structures were thereafter solved and the general principles of the binding interactions between peptides and MHC were established. MHC Class I molecules typically bind peptides of 8-10 residues in length in an extended conformation in the peptide binding groove, and specific amino acids comprise pockets that accommodate the corresponding side chains of the anchor residues of the presented peptides [5-8].

We identified previously two HLA-A*0201-restricted CTL 10-mer epitopes in influenza H5N1 virus HA (HA 205-214), RI-10 (RLYQNPTTYI) and KI-10 (KLYQNPTTYI) [9], which locate on the head of HA (Figure 1). They originate from different H5N1 virus strains and differ only slightly from each other: thus, in RI-10, the first amino acid residue is arginine (R), whereas in KI-10, it is lysine (K). We solved the respective crystal structures of RI-10 and KI-10 in complex with HLA-A*0210; these revealed that although RI-10 and KI-10 have very similar

2

primary sequences, they nevertheless display conformations that are obviously different from each other (Figure 1). However, it is unknown whether the different conformations of the two peptide may impact their antigenicity, the primary consideration in vaccine design.

Although mutations both in peptides and MHC molecules leading to the change of T cell response has been reported, how substitutions between very similar residues like Arg and Lys at N-terminal of peptides could affect the peptide immunogenicity remains unclear. Recently, structural dynamics study by molecular dynamics (MD) simulation on pMHC structures suggested that structural flexibility of the peptides can have a role in peptide immunogenicity [10, 11]. In the present study, we carry out MD simulations on RI-10-HLA-A*0201 and KI-10-HLA-A*0201 complexes in order to examine whether they also have different structural dynamic properties. Our results reveal that the slight difference in the first residue of these two peptides does lead to different structural dynamics of the two peptides in the antigen binding cleft, which were related to their different antigenicity.

Results and discussion

Molecular Mechanics/Poisson-Boltzmann Surface Area (MM/PBSA) calculations.
The peptides RI-10 and KI-10 have only a slight difference in their primary sequences: the first residue of RI-10 is arginine (Arg), whereas the first residue of KI-10 is lysine (Lys). Arg and Lys are both basic amino acids, and the difference between these two amino acids lies in their side-chain terminus. The side-chain terminus of Arg is a guanidine, whereas that of Lys is an amidogen. Nevertheless, the overall conformations of RI-10 and KI-10 show obvious differences in the respective crystal structures of the two peptides in complex with HLA-A*0201. The root mean square deviation (RMSD) between the two peptides is 1.482 Å. The conformational difference between the two peptides lies mainly in the central residues (P4-P8). For these residues, both the positioning of the main chain and the orientation of the side chain differ between the two peptides (Figure 1).

We carried out 100 ns MD simulations on both RI-10-HLA-A*0201 and KI-10-HLA-A*0201 complexes. To allow more extensive conformational sampling, we performed the simulations three time. The RMSD were quite converged for the two complexes, especially the last 50 ns of the simulations (Figure S1A). We concatenated the last 50 ns trajectories of the three simulations on each pMHC

complexes respectively into single 150 ns trajectories for MM/PBSA calculation and most analysis in this article. In order to calculate binding free energy, we also performed simulations on the empty HLA-A*0201 molecules without the peptides and the free peptides extracted from the complexes. The simulations on the empty HLA-A*0201 molecules were also done three times. The RMSD values of the empty HLA-A*0201 molecules were as converged as the pMHC complexes (Figure S1B) and we also concatenated the last 50 ns trajectories of the three simulations into single 150 ns trajectories for MM/PBSA calculation. The RMSD of the free peptides were difficult to converge. For KI-10, RMSD became relative converged after 100 ns, but the fluctuation is larger than that of the pMHC complex and the empty MHC; for RI-10, the RMSD became quite converged after 250 ns (Figure S1C). We used the last 150 ns trajectories of the two free peptides for MM/PBSA calculation. When inspecting the representative structures (the structures most similar to the average structures) of these free peptide of the last 150 ns, we found that both of them didn't show extended conforms as in the peptide binding cleft of HLA-A*0201 molecule (The radius of gyration of RI-10 and KI-10 in their bound state were 8.72 and 8.64, respectively); instead, their backbone bent and the N- and C-terminal came close to each other and form ring-like structures (The radius of gyration of RI-10 and KI-10 in their free state were 6.85 and 6.23, respectively) (Figure S2). For RI-10, the Arg1 formed intensive polar contact (salt bridges or hydrogen bonds with Ile10; while for KI-10, the structure of the bended ring were mainly stabilized by a hydrogen bond formed between Leu2 and Tyr9.

We performed MM/PBSA calculations to compare the binding free energies for the binding of RI-10 and KI-10, respectively, to HLA-A*0201. The concatenated 150 ns trajectories of the pMHC complexes, the empty MHC molecules, and the last 150 ns trajectories of free peptides were used for the calculation. All energy terms of each species were listed in table S1. If entropy was not considered, the binding free energies for the binding of RI-10 and KI-10 to HLA-A*0201 were -180.55 and -22.90 kJ/mol, respectively, indicating that the free energy for the binding of RI-10 to HLA-A*0201 was much higher than that for the binding of KI-10 (Table S1). It should be noted that both coulombic and van der Waals energies were favorable for the binding, but the polar solvation energy was unfavorable. Non-polar solvation terms (ΔG_{nps}), which corresponded to the burial of solvent-accessible surface area (SASA) upon binding, made a small favorable contribution. The difference between the binding free energies for RI-10 and KI-10 arose mainly from coulombic energy; the electrostatic interactions between these two peptides and HLA-A*0201 were therefore significantly different.

Here the MM/PBSA method did not include entropy. Entropy can be calculated by quasi-harmonic analysis [12]. However, it is highly debated whether including entropy can indeed improve the binding free energy estimates and entropy is often neglected in computational free energy calculations[13, 14]. Entropy loss (ΔS) opposes the peptide binding, so when the entropy term was included, the relative smaller relative binding free eneregy of KI-10 to HLA-A*0201 calculated in table S1 became positive (10.2 kJ/mol). The entropy loss of RI-10 binding to HLA-A*0201 was larger than that of KI-10 binding to HLA-A*0201. Even thus, the binding free energy of RI-10 to HLA-A*0201 was still high (-106.15 kJ/mol) (Table S2).

The thermal stability of RI-10-HLA-A*0201 was higher than that of KI-10-HLA-A*0201. Thermal denaturation curves for RI-10-HLA-A*0201 and KI-10-HLA-A*0201 were determined by monitoring the loss of secondary structure, using circular dichroism (CD). The initial loss of secondary structure is attributable to the loss of the peptide, and to the unfolding of the Heavy chain (HC), and a second transition observed in the denaturation curves and beginning close to 85 ℃ corresponds to the unfolding of β2m. [15] The mid-points of the transitions (melting temperatures, T_m) were 58 ℃ for RI-10-HLA-A*0201 and 50 ℃ for KI-10-HLA-A*0201 (Figure 2), indicating that the thermal stability of RI-10-HLA-A*0201 was higher than that of KI-10-HLA-A*0201. The T_m value as measured by CD is proportional to the binding free energy for the binding of the peptide to the MHC [16]. It can therefore be concluded that the free energy for the binding of RI-10 to HLA-A*0201 was higher than that for the binding of KI-10.

Structural fluctuation of RI-10-HLA-A*0201 is lower than that of KI-10-HLA-A*0201. We next examined the structural fluctuation of these the pMHC complexes. The root mean square fluctuations (RMSF) for both the RI-10 and KI-10 peptides and for the HLA-A*0201 heavy chain (HC) were measured. Surprisingly, the results showed that the RMSF values for all of the individual residues of KI-10 peptide were significantly higher than the corresponding values for RI-10 peptide ($p < 0.05$, student's t-test) (Figure 3A), although the temperature (B) factors for the corresponding residues of the two peptides were very similar in the crystal structures. RMSD-based clustering analysis showed that the conformations of KI-10-HLA-A*0201 during the MD simulations could be divided into 6 clusters, and the percentage of these clusters were 48.4 %, 14.4 %, 14.1 %, 11.5 %, 8.8 % and 2.8 %. The main chain shapes of KI-10 peptide in the representative complex structures (the structure most close to the average structure) of their respective clusters were obviously different from each other. In contrast, the conformations of RI-10-HLA-A*0201 were divided into four clusters, but most conformations belongs to one big cluster. The percentage of these four clusters were 94.5 %, 3.8 %, 1.0 %,

0.7 %. The main chain shapes of the RI-10 peptide in the representative structures of all these clusters were very similar (Figure 3B). These results further conformed that KI-10 was more flexible than RI-10 in cleft of HLA-A*0201 during the MD simulations.

When comparing the RMSF values of individual residues in peptide bound HLA-A*0201 heavy chain (HC) of the two complexes, we found that the RMSF values of every residues of the KI-10-HLA-A*0201 HC were also higher than those of RI-10-HLA-A*0201 HC, and the largest difference for the RMSF values of HC between these two complexes locate on the α1- and α2-domain, including the α1- and α2-helices (residues 53-84 and 138-179, respectively) on the top surface of pMHC molecules which constitute the potential TCR docking sites (Figure 3C and S5).

In order to examine the effects of peptide binding on the fluctuation of HLA-A*0201, we also calculated the RMSF values of individual residues of HLA-A*0201 HC based on the simulation trajectories of the empty HLA-A*0201 molecules extracted from RI-10-HLA-A*0201 and KI-10-HLA-A*0201 complexes. RMSF values of most corresponding residues of the two empty HLA-A*0201 molecules were very similar, so the differences between the RMSF values these corresponding residues were close to zero, and the average of the RMSF differences for the 275 residues of HLA-A*0201 HC were -0.02 Å (Figure 3D). In contrast, the differences between RMSF values of most residues in RI-10 and KI-10 bound HLA-A*0201 were higher than 0.5 Å and the average of the RMSF differences were 0.65 Å (Figure 3C). Furthermore, when comparing the RMSF of individual residues of the peptide bound and empty HLA-A*0201 HC from the same complex, it was shown that RI-10 binding slightly increased RMSF values of most residues of HLA-A*0201 HC, and the average RMSF differences of these 275 residue was 0.29; in contrast, KI-10 binding remarkably increased the RMSF values of all residues of HLA-A*0201 HC, and the average RMSF differences of the 275 residue of HLA-A*0201 HC was 0.96 (Figure S3). These results suggested that binding of RI-10 and KI-10 differently affected the fluctuations of HLA-A*0201: KI-10 more significantly increased the fluctuations of HLA-A*0201 than KI-10.

Conformational bundles of both the peptide and the HLA-A*0201 HC representing the conformations in the 150 ns concatenated MD trajectories of KI-10-HLA-A*0201 complex were obviously broader than those in RI-10-HLA-A*0201 (figure S4A and S4B), which also suggested that the fluctuation of those structural regions was higher in KI-10-HLA-A*0201 complex than in RI-10-HLA-A*0201.

During its interaction with the pMHC, TCR CDR3 loop frequently participates in peptide-mediated interactions, whereas the CDR1 and CDR2 loops make contact with the MHC [17, 18]. According to the TCR-pMHC class I (pMHCI) complex structures that have been solved, TCRs usually dock above the pMHCI molecules in a diagonal orientation and the points at which docking occurs on the pMHC ligands are usually two exposed areas on the upper faces of MHC helices, centered around α1 69 and α2 158 [19]. And in all known TCR–pMHCI structures, the TCR makes contact with three MHC positions, namely 65, 69, and 155 (a so-called "restriction triad"). Two of these potential TCR interacting residues, Glu63 and Gln155 are among those which showed the largest RMSF difference between KI-10-HLA-A*0201 and RI-10-HLA-A*0201 complex (Figure 3C). So our RMSF results suggested that the TCR recognizing interface of KI-10-HLA-A*0201 processed higher fluctuation than that of RI-10-HLA-A*0201.

Different atom contact patterns between RI-10 and K-10 with HLA-A*0201 lead to the different structural dynamics observed for the two pMHC complexes. Our next step was to analyze the underling mechanisms that gave rise to the differences between structural dynamics of the two pMHC complexes. We first examined the atom contacts between the first residues, Arg1 or Lys1 of the two peptides with HLA-A*0201 in their concatenated 150 ns trajectories. As shown in the distribution of the numbers of HLA-A*0201 residues that made atom contacts with Arg1 of RI-10 or Lys1 of KI-10, Arg1 of RI-10 obviously contacted more resides in HLA-A*0210 than Lys1 of KI-10: the average count of HLA-A*0201 residues that made atom contacts with Arg1 of RI-10 was 7.9, while the count of HLA-A*0201 residues that made atom contacts with Lys1 of KI-10 was 4.4 (Figure 4A). When aligning the representative structures (the structures that were most similar to the average structures) of the 150 ns trajectories of the two pMHC complexes, we found that the positioning of the first residues of RI-10 and KI-10 is significant different: Arg1 of RI-10 remained binding in pocket A of HLA-A*0201 as in the crystal structure, while Lys1 of KI-10 floated upwards and left its initial binding pocket (Figure 4B). In the representative structures of the 150 ns trajectory, RI-10 made atom contacts with Tyr7, Tyr59, Gly62, Glu63, Thr143, Tyr159 Trp167 and Tyr171 of HLA-A*0201; in contrast, Lys1 of KI-10 made atom contacts only with Tyr59, Gly62, Glu63, Trp167 and Tyr171 of HLA-A*0201 (Figure 4C and D).

A critical difference is that N-terminal residue Arg1 of RI-10 forms salt bridges with Glu63 of HLA-A*0201 (Figure 4E) , while KI-10 does not form any salt bridge with HLA-A*0201 in the representative structures of the 150 ns concatenated trajectories.

The salt bridges could be formed between the NH1, NH2 or NE atom of Arg1 in RI-10 and the OE1 or OE2 atom of Glu63 in HLA-A*0201. The NE atom of Arg1 of RI-10 formed a salt bridge with the OE2 atom of HLA-A*0201 Glu63 in 97.0 % snapshots of the 150 ns concatenated trajectory of RI-10-HLA-A*0201. Similarly, the NH2 atom of RI-10 Arg1 formed a salt bridge with the OE2 atom of HLA-A*0201 Glu63 during 96.2 % snapshots in the concatenated trajectory. In one of the 100 ns simulations, RI-10-Arg1-NE···OE2-Glu63-HLA-A*0201 HC and RI-10-Arg1-NH2···OE2-Glu63-HLA-A*0201 HC salt bridge formed shortly after the initiation of the simulation and sustained till the end of the simulation (Figure 4F).

In addition to the different atom contact patterns between the first residue of RI-10 or KI-10 with HLA-A*0201, the atom contact patterns between the whole RI-10 or KI-10 peptide with HLA-A*0201 were different. Here we analyzed the hydrogen bonds between the peptides and HLA-A*0201 in their respective 150 ns concatenated trajectories. As shown in table S3, the pattern of the hydrogen bond network formed between RI-10 and HLA-A*0201 was very different from that formed between KI-10 and HLA-A*0201. Firstly, O atom of Arg1 of RI-10 formed a stable hydrogen bond with OH atom of Tyr159 of HLA-A*0201 heavy chain (HC) (occupancy being 79.4 %). In contrast, the hydrogen bond formed between O atom of Lys1 of KI-10 and OH atom of Tyr159 of HLA-A*0201 HC was relatively unstable (occupancy being 31.4 %). Besides, N atom of Arg1 of RI-10 formed hydrogen bonds with OE1 and OE2 atom of Glu63, OH atom of Tyr171 and Tyr7, and NE1 atom of Trp167 of HLA-A*0201 HC (occupancy ranging from 9.9 to 20.4), while N atom of KI-10 only formed a hydrogen bond with OE1 atom of Glu63 of HLA-A*0201 HC (occupancy being 32.3 %). N atoms of RI-10 formed hydrogen bonds with OE1 and OE2 atoms with Glu63 of HLA-A*0201 HC (occupancy being 28.3 % and 11.5 %, respectively), while N atom of KI-10 Leu2 only formed a hydrogen bond with OE1 atom of Glu63 of HLA-A*0201 HC with occupancy being 17.7 %. Tyr3 of RI-10 formed a very stable hydrogen bond with Try99 of HLA-A*0201 HC with occupancy being 87.9%, but Tyr3 of KI-10 didn't form any hydrogen bond with HLA-A*0201; Gln4 of RI-10 formed a hydrogen bond with Lys66 of HLA-A*0201 HC with occupancy being 27.3 %, and again Gln4 of KI-10 didn't formed any hydrogen bond with HLA-A*0201. Asn5, Pro6 and Thr7 of RI-10 didn't form hydrogen bonds with HLA-A*0201; Asn5 and Thr7 of KI-10 forms hydrogen bonds with Arg97 and Thr73, but the occupancies were low (10.6 and 11.6, respectively). Thr8 of RI-10 formed a hydrogen bond with HLA-A*0201 HC with an occupancy of 41.2 %, while Thr8 of KI-10 didn't form any hydrogen bond with HLA-A*0201. Tyr9 of RI-10 formed a very stable hydrogen bond with HLA-A*0201 HC with an occupancy of 87.2 %, but Tyr9 of KI-10 didn't form any stable hydrogen bond with HLA-A*0201. Ile10 of RI-10 formed six hydrogen bonds with HLA-A*0201 HC, and four of these hydrogen bonds also exited between Ile10 of KI-10 and HLA-A*0201 HC. Among these four hydrogen bonds, only one in RI-10-HLA-A*0201 had an occupancy slightly lower

8

than in KI-10- HLA-A*0201: it was formed with the OT1 atom of Ile10 of the peptide and OH atom of Tyr84 of HLA-A*0201 HC (occupancy being 22.6 % in RI-10-HLA-A*0201 vs 32.0 % in KI-10-HLA-A*0201), while other three all had an occupancy higher in RI-10-HLA-A*0201 than in KI-10-HLA-A*0201). Generally speaking, the number and stability (occupancy) of the hydrogen bonds formed between RI-10 and HLA-A*0201 were obviously higher than those between KI-10 and HLA-A*0201. So the data suggested that RI-10 formed more extensive hydrogen bond network with HLA-A*0201 compared with KI-10.

The difference in hydrogen bond networks formed between two peptides and HLA-A*0201 was consistent to their difference in the molecular dynamics described above. The higher binding free energy to HLA-A*0201 and lower fluctuation of RI-10 compared with KI-10 can be attributed at least in part to the weaker hydrogen bond networks. And we speculate that the different hydrogen bond networks between the two peptides and HLA-A*0201 may arise from the different atom contact patterns between the first residues of RI-10 and KI-10. The link between the atom interactions between the first residues of the peptides and the fundamentally different structural dynamics of the two peptides and the whole pMHC molecules can be explained by allosteric interactions.

Theories of allosteric interactions or indirect interactions were initially developed to explain the mechanisms by which a regulatory ligand (such as an enzyme feedback inhibitor) controls the state of activity of a biologically active site, such as an enzyme catalytic site, despite being structurally different from the active-site substrate. Regulatory effectors and substrates were proposed to bind to their target protein at topographically "distinct sites". Thus, a small molecule binding event at one site of a protein can propagate a signal to a different site and trigger a change in structure and biochemical function there [20-22]. Recently, the classic allosteric theory has been extended and the observations that changes in protein intrinsic motions and the dynamic profile of molecular fragments play a powerful role in modulating chemical behavior give rises a concept of "nonclassical allostery" or "dynamic allostery", which emphasizes the distinctively different underlying mechanism of remote controlling the chemical property [23, 24]. Examples of remote controlling in the MHC system have been reported in which tapasin regulates peptide binding to HLA-B*44:02 by altering the dynamics state of its F pocket [25].

In our cases, the N-termini of both RI-10 and KI-10 are buried in the antigen binding cleft of HLA-A*0201 and therefore inaccessible to TCR recognition. However, their different interaction with HLA-A*0201 molecule, especially the salt bridges that exist between Arg1 of RI-10 and HLA-A*0201 but not Lys1 of KI-10, led to different dynamics of N-terminal of the two peptides. The signal of the slightly different local atom interactions between the first residue of peptide with HLA-A*0201 then

transmitted through the standard peptidyl building block to the whole peptide, thus the interactions between the other residues of the peptide (residue 2-10) and HLA-A*0201 were affected, and thus HLA-A*0201 molecules of the two complexes showed different dynamics property. Specifically, two residues (Glu63 and Gln155) in the potential TCR recognition sites (the "restriction triad") were also peptide binding resides (Figure S5). This may explain why the slight sequence difference in the peptides can lead to different dynamics in MHC and TCR recognition.

Possible connection between different structural dynamics of RI-10 and KI-10 peptides and their antigenic potency. The comparative MD simulation study described above revealed different dynamics for the RI-10-HLA-A*0201 and KI-10-HLA-A*0201 complexes, but it was not clear how this difference might influence their immunological properties. We extracted all the 45 HA sequences of H5N1 virus isolated from Chinese human from 2003 till April 10, 2014 in Influenza Research Database (http://www.fludb.org/brc/home.spg?decorator=influenza). By an alignment of these HA sequences, it became clear that although the number of avian isolates containing RI-10 is comparable to the number containing KI-10, the majority of human isolates in China contain KI-10. Amongst the 45 human H5N1 virus isolates, 42 contained KI-10, and only three contained RI-10 (Figure S6). Since the numbers of RI-10- and KI-10-containing avian-isolated H5N1 strains are comparable, it can be assumed that human exposure to these two kinds of avian strains should be equal. Nevertheless, the KI-10-containing strains obviously dominate the human isolates; a possible explanation would be that KI-10-containing strains more readily cause detectable disease in humans.

To elucidate whether the difference in frequency of occurrence between RI-10- and KI-10-containing H5N1 virus strains is related to the different immunogenic potency of the two peptides, we immunized HLA-A*0201/K^b transgenic mice with the two peptides and evaluated the CTL response by counting IFN-γ producing cells, using an enzyme-linked immunospot (ELISPOT) assay. As shown in Figure 5, the splenocytes isolated from the control group of mice that had not been immunized with either of these two peptides *in vivo* did not generate an obvious CTL response, even when they were stimulated with RI-10 or KI-10 *in vitro*. In contrast, the splenocytes isolated from the mice that had been immunized *in vivo* with RI-10 produced a high CTL response; and the response became significantly higher ($p<0.05$, student's test) when they were stimulated with RI-10 (but not KI-10) *in vitro*. Immunization *in vivo* with KI-10 also produced a CTL response, but the response was significantly lower than that produced by RI-10 immunization. Surprisingly, KI-10 stimulation did not significantly ($p>0.05$, student's test) increase the response in splenocytes isolated from KI-10-immunized mice; however, RI-10 stimulation did significantly ($p<0.05$, student's test) increase the response in these splenocytes.

10

The majority of human class I MHC (HLA)-restricted peptides studied to date are 9-mer and 10-mer peptides, and their anchor residues are usually P2 and C-terminal residues [26, 27]; P1 and P3 residues have been identified as secondary or auxiliary anchor residues that fine-tune peptide recognition [28]. Nevertheless, the importance of the P1 residue from an energetics standpoint was recognized in some early studies. Thus Bouvier et al. showed that, in the complex formed between the influenza virus peptide (GL9, GILGFVFTL) and HLA-A*0201, the T_m of the complex decreased by 22 °C when the N-terminal amino group of GL-9 was replaced by a methyl group and the hydrogen bonds formed between the N-terminal residue and HLA-A*0201 were blocked, indicating a large decrease in the stability of the complex [29]. Removal of the P1 residue of the peptide was also shown to lead to a large decrease in the thermal stability of the pMHC complex [15]. In the present study, we demonstrated that a very small alteration in the P1 residue of the peptide could lead to significantly different binding free energy and thermal stability of pMHC complexes.

We found that the relative binding free energy for KI-10 was much lower than that of RI-10 in their interaction with HLA-A*0201 and the electrostatic interactions between KI-10 and HLA-A*0201 were much weaker than those between RI-10 and HLA-A*0201. As a result, the KI-10-HLA-A*0201 complex was more stable than RI-10-HLA-A*0201, suggesting that KI-10 would have a lesser chance of being sampled by HLA-A*0201 in the endoplasmic reticulum, presented and elicits a CTL response.

KI-10 was significantly more flexible than RI-10 while in the peptide binding cleft of HLA-A*0201. Although flexibility of the peptide and the MHC molecule was reported to be important for the stability of the complementary binding between pMHC and TCR in some studies [30, 31], in many cases, excessive peptide flexibility was shown to be unfavorable for eliciting an immune response [11, 32, 33]. This is consistent with our finding that the regions aa 55-77 in α1-helix and aa142-167 in α2-helix in the KI-10-HLA-A*0201 complex showed higher flexibilities than the corresponding regions in RI-10-HLA-A*0201, and that the regions of HLA-A*0201 most sensitive to peptide flexibility variation are in the α1 and α2-helix. As shown in many studies, a greater flexibility of the aa sequences in the potential TCR recognition interface, including the peptide and the potential TCR docking sites on MHC, would lead to a decrease in entropy loss during TCR binding which is unfavorable to TCR recognition. ELISPOT assays of the peptide-immunized HLA-A*0201/K[b] Tg mice presented in this study suggested that the higher flexibility

of the TCR recognition interface in KI-10-HLA-A*0201 led to a loss of antigenic potency of KI-10.

CTL response has been proposed to play a protective role against influenza virus infection [34, 35] and its study may provide clues to understanding the barriers that prevent cross-species transmission of the H5N1 viruses. The HLA-A*0201 and its closely related HLA-A2 supertype alleles, including HLA-A*0203, HLA-A*0206 and HLA-A*0207 are very common in the human population (approximately 50%) and an adequate HLA-A2-restricted CTL response may play a significant role in the defence against H5N1 viruses jumping from avian to human. Although the HLA-A2-restricted CTL epitopes in the influenza virus are considered to be dominated by the conserved M1 (58-66) peptide [36, 37], our studies with HLA-A*0201/K^b Tg mice showed that RI-10, the H5-specific HLA-A*0201-restricted CTL epitope, elicited a robust CTL response which was much higher than that induced by M1 (58-66) [9]. If the dosage of RI-10-mediated CTL response plays a dominant role in getting rid of H5N1 virus infected cells during the latent phase of infection so as to prevent the development of detectable disease symptoms, the substitution of Lys in RI-10 with Arg1 which resulted in a loss of antigenic potency, is a possible explanation for KI-10 containing H5N1 virus strains dominating the virus strains isolated from human patients. Our results, therefore, highlight the potential for altering the molecular dynamics of the peptide-pMHC interface as a novel mechanism of virus immune escape.

The basic merit of the results presented in this study is for vaccine design. Although identifying determinants antigenicity of epitopes by numerous experimental biophysical methods has been a focus of research for many years, the importance of computational simulation as an implements to experiments is becoming more and more recognized. In many cases, the computational results are highly correlated with experiments, so computation-aided vaccine design could help reduce the cost and risk of experiments. Our results that a very slight change in epitope sequences giving rise to dramatic difference in structural dynamics and antigenicity suggest that caution must be taken when selecting very similar vaccine candidates. Recently, Ortoleva's group proposed a fluctuation-immunogenicity hypothesis based on their MD simulations on the human papillomavirus (EVP) vaccines of different L1 protein assemblies [11, 38-40]. Our observation seem to obey Ortoleva's theory: higher structural flexibility or structural fluctuation of epitopes is related to lower antigenicity. Although the fluctuation-immunogenicity hypothesis is derived from data of antibody binding, we show that it can also apply to CTL response. So this might be a general aspect in immune recognition.

Experimental
Molecular dynamics simulations
The published crystal structures of RI-10-HLA-A*0201 (PDB ID: 3MGO) and KI-10-HLA-A*0201 (PDB ID: 3MGT) were used for the simulations. Both crystal structures contain four pMHC complexes in the asymmetric unit. Since these four complexes in the asymmetric unit are structurally identical, we performed simulations on just one of them (the complex composed of chain A, B and C). MD simulations were performed using the NAMD 2.9 MD software package [41] and the CHARMM22 protein force field [42]. The structures were solvated with waters (TIP3P model) and 0.15 M NaCl. The minimum distance from the protein to the water box boundaries was 0.8 nm for both of the two systems. The two systems were firstly subjected to energy minimization. For all simulations a timestep of 2 fs was used as well as periodic boundary conditions and PME for electrostatics. The systems were heated to 310 K with the Cα atoms constrained for 1 ns. The systems were equilibrated for another 1 ns without constraints before the production runs used for analysis. Parameters for all simulations were: temperature 298 K, switching distance 10 Å, switching cutoff 12 Å, pairlist distance 14 Å , Langevin damping coefficient 1 ps, Langevin pressure control with a target pressure of 1.01325 bar. In order to calculate binding free energy of the peptides to HLA-A*0201, the coordinates of the peptides and the empty HLA-A*0201 were extracted from the crystal structures of the two pMHC complexes respectively and MD simulations were performed under the same conditions as the pMHC complexes as described above.

Binding free energy calculation. Binding free energy of the peptides to HLA-A*0201 was calculated by MM/PBSA method. This method is based on an analysis of MD trajectories using a continuum solvent approach and approximates the "average" free energy of a state as

$$\langle G \rangle = \langle E_{MM} \rangle + \langle G_{PBSA} \rangle - T \langle S_{MM} \rangle \tag{1}$$

where $\langle E_{MM} \rangle$ is an average molecular mechanical energy that typically includes bond, angle, dihedral angle, improper, van der Waals and electrostatic terms from a regular force field. $\langle G_{PBSA} \rangle$ includes polar and non-polar solvation energy. $\langle S_{MM} \rangle$ is solute entropy. The binding free energy can be calculated by evaluation of the terms in equation (1) for the pMHC complex, the receptor (empty HLA-A*0201 molecule here) and the ligand (the peptide) according to

$$\langle \Delta G_{bind} \rangle = \langle G_{complex} \rangle - \langle G_{receptor} \rangle - \langle G_{ligand} \rangle \tag{2}$$

For MM/PBSA calculation, all the energy terms including intramolecular terms or conformational terms (bond, angle, dihedral angle and improper), the nonbond terms (van der Waals and electrostatic terms), the polar and non-polar solvation energy

terms, and the sum of all these terms (the total free energy) of the each species (the pMHC complex, the empty MHC and the peptide) were calculated for each snapshot from their respective MD trajectories and averaged. The binding free energy then were obtained according to equation (2). All the energy terms of intramolecular and nonbond terms were calculated by NAMD energy plugin of VMD program [43], and polar and non-polar solvation energy terms were calculated by APBS program [38]. The entropy was calculated by Schlitter method [44] coded in Carma program [45].

Circular dichroism (CD). Thermal stability of peptide-MHC complexes was monitored by CD spectroscopy using a Pistar π-180 instrument (Applied Photophysics Ltd, UK). Solution conditions were 20 mM Tris and 50 mM NaCl (pH 7.4). Protein concentrations were 0.15 mg/ml. The spectrum between 260 nm and 190 nm indicated a predominantly β-sheet conformation. Temperature denaturation was monitored at the minimum of 218 nm between 20 °C and 90 °C, using a gradient of 1 °C/min. Scans were repeated twice with fresh protein and the data points were averaged. The data in the transition region were fitted to an eight-order polynomial equation, and the apparent T_m was determined from the maximum of the first derivative of the fitted curve [15].

Immunization of HLA-A*0201/K^b transgenic mice, and ELISPOT assay. Female HLA-A*0201/K^b Tg mice (purchased from the Model Animal Resource Center of Nanjing University, China), 6–8 weeks old, were immunized subcutaneously at multiple sites with a mixture of 100 μg peptides and incomplete Freund's adjuvant (Sigma, USA) three times at intervals of 10 days. The injection volume was adjusted to 200 μl for each animal. Ten days after the last immunization, the mice were sacrificed and the spleens were recovered, dispersed with a syringe plunger and passed through cell strainers. Erythrocytes were lysed with 0.83 % NH_4Cl lysis solution (0.83 % NH_4Cl, 0.26% Tris–HCl, pH 7.2). Splenocytes were then washed and resuspended in RMPI 1640 medium supplemented with 10% fetal bovine serum (Life Technologies, China). The peptide-induced CTL response was evaluated by detecting IFN-γ-producing cells, using an ELISPOT assay kit (Dakewe, China). Briefly, 3×10^5 murine splenocytes were seeded into 96-well plates pre-coated with anti-IFN-γ capture antibody in duplicate wells. To stimulate the effector cells, 10 μM peptide was added. The plates were incubated at 37 °C for 16 h. The cells were then removed and the plate was processed according to the manufacturer's instructions. The colored spots, representing epitope-specific IFN-γ-producing T cells, were counted using an automatic ELISPOT reader (Biosys, Germany). The animal experiments were approved by the Animal Welfare Committee, Institute of Microbiology, Chinese Academy of Sciences.

Conclusions

In the present study, we show that slight sequence change in the peptide presented by a MHC molecule can lead to dramatic alternation in structural dynamics of the whole pMHC complex, which is a critical determinant of antigenicity of the peptide. Our results also suggest the signal of slight local changes of atom contacts can diffuse to the whole protein molecule and result in significant changes of the structural dynamics in the whole molecules.

Abbreviations

MHC, major histocompatibility complex; TCR, T cell receptor; β2m, β2 microglobulin; HC: heavy chain; RMSF, The root mean square fluctuations; CD, circular dichroism; MM/PBSA, Molecular Mechanics/Poisson-Boltzmann Surface Area; HA, Hemagglutinin.

Bibliographic references

1. J. S. Blum, P. A. Wearsch and P. Cresswell, *Annu Rev Immunol*, 2013, 31, 443-473.
2. P. J. Bjorkman, M. A. Saper, B. Samraoui, W. S. Bennett, J. L. Strominger and D. C. Wiley, *Nature*, 1987, 329, 512-518.
3. P. J. Bjorkman, M. A. Saper, B. Samraoui, W. S. Bennett, J. L. Strominger and D. C. Wiley, *Nature*, 1987, 329, 506-512.
4. D. R. Madden, *Annu Rev Immunol*, 1995, 13, 587-622.
5. M. G. Rudolph, R. L. Stanfield and I. A. Wilson, *Annu Rev Immunol*, 2006, 24, 419-466.
6. C. S. Hee, S. Gao, B. Loll, M. M. Miller, B. Uchanska-Ziegler, O. Daumke and A. Ziegler, *Plos Biol*, 2010, 8.
7. K. J. Smith, S. W. Reid, K. Harlos, A. J. McMichael, D. I. Stuart, J. I. Bell and E. Y. Jones, *Immunity*, 1996, 4, 215-228.
8. D. R. Madden, D. N. Garboczi and D. C. Wiley, *Cell*, 1993, 75, 693-708.
9. Y. Sun, J. Liu, M. Yang, F. Gao, J. Zhou, Y. Kitamura, B. Gao, P. Tien, Y. Shu, A. Iwamoto, Z. Chen and G. F. Gao, *J Gen Virol*, 2010, 91, 919-930.
10. I. J. General, Y. Liu, M. E. Blackburn, W. Mao, L. M. Gierasch and I. Bahar, *PLoS Comput Biol*, 2014, 10, e1003624.
11. F. K. Insaidoo, O. Y. Borbulevych, M. Hossain, S. M. Santhanagopolan, T. K. Baxter and B. M. Baker, *The Journal of biological chemistry*, 2011, 286, 40163-40173.
12. J. Wereszczynski and J. A. McCammon, *Quarterly reviews of biophysics*, 2012, 45, 1-25.
13. T. Hou, J. Wang, Y. Li and W. Wang, *J Chem Inf Model*, 2011, 51, 69-82.
14. D. Spiliotopoulos, A. Spitaleri and G. Musco, *PLoS One*, 2012, 7, e46902.
15. A. R. Khan, B. M. Baker, P. Ghosh, W. E. Biddison and D. C. Wiley, *J Immunol*, 2000, 164, 6398-6405.
16. C. S. Morgan, J. M. Holton, B. D. Olafson, P. J. Bjorkman and S. L. Mayo, *Protein Sci*, 1997, 6, 1771-1773.

17. K. C. Garcia, J. J. Adams, D. Feng and L. K. Ely, *Nature Immunology*, 2009, 10, 143-147.

18. M. K. Gilson and H. X. Zhou, *Annu Rev Biophys Biomol Struct*, 2007, 36, 21-42.

19. S. Gras, S. R. Burrows, S. J. Turner, A. K. Sewell, J. McCluskey and J. Rossjohn, *Immunol Rev*, 2012, 250, 61-81.

20. J. P. Changeux and S. J. Edelstein, *Science*, 2005, 308, 1424-1428.

21. B. M. Martins and P. S. Swain, *PLoS Comput Biol*, 2011, 7, e1002261.

22. M. Merdanovic, T. Monig, M. Ehrmann and M. Kaiser, *ACS chemical biology*, 2013, 8, 19-26.

23. A. Singharoy, A. Polavarapu, H. Joshi, M. H. Baik and P. Ortoleva, *J Am Chem Soc*, 2013, 135, 18458-18468.

24. J. P. Changeux, *Nature reviews. Molecular cell biology*, 2013, 14, 819-829.

25. M. A. Garstka, S. Fritzsche, I. Lenart, Z. Hein, G. Jankevicius, L. H. Boyle, T. Elliott, J. Trowsdale, A. N. Antoniou, M. Zacharias and S. Springer, *Faseb Journal*, 2011, 25, 3989-3998.

26. X. Rao, A. I. Costa, D. van Baarle and C. Kesmir, *J Immunol*, 2009, 182, 1526-1532.

27. P. J. Bjorkman and P. Parham, *Annu Rev Biochem*, 1990, 59, 253-288.

28. P. A. Kollman, I. Massova, C. Reyes, B. Kuhn, S. Huo, L. Chong, M. Lee, T. Lee, Y. Duan, W. Wang, O. Donini, P. Cieplak, J. Srinivasan, D. A. Case and T. E. Cheatham, 3rd, *Acc Chem Res*, 2000, 33, 889-897.

29. M. Bouvier and D. C. Wiley, *Science*, 1994, 265, 398-402.

30. W. F. Hawse, S. De, A. I. Greenwood, L. K. Nicholson, J. Zajicek, E. L. Kovrigin, D. M. Kranz, K. C. Garcia and B. M. Baker, *Journal of Immunology*, 2014, 192, 2885-2891.

31. O. Y. Borbulevych, K. H. Piepenbrink, B. E. Gloor, D. R. Scott, R. F. Sommese, D. K. Cole, A. K. Sewell and B. M. Baker, *Immunity*, 2009, 31, 885-896.

32. C. F. Reboul, G. R. Meyer, B. T. Porebski, N. A. Borg and A. M. Buckle, *PLoS Comput Biol*, 2012, 8, e1002404.

33. T. Pohlmann, R. A. Bockmann, H. Grubmuller, B. Uchanska-Ziegler, A. Ziegler and U. Alexiev, *Journal of Biological Chemistry*, 2004, 279, 28197-28201.

34. E. O'Neill, S. L. Krauss, J. M. Riberdy, R. G. Webster and D. L. Woodland, *J Gen Virol*, 2000, 81, 2689-2696.

35. W. T. Gao, A. C. Soloff, X. H. Lu, A. Montecalvo, D. C. Nguyen, Y. Matsuoka, P. D. Robbins, D. E. Swayne, R. O. Donis, J. M. Katz, S. M. Barratt-Boyes and A. Gambotto, *Journal of Virology*, 2006, 80, 1959-1964.

36. M. Terajima and F. A. Ennis, *J Virol*, 2012, 86, 10258; author reply11259-10260.

37. C. Wu, D. Zanker, S. Valkenburg, B. Tan, K. Kedzierska, Q. M. Zou, P. C. Doherty and W. Chen, *Proc Natl Acad Sci U S A*, 2011, 108, 9178-9183.

38. N. A. Baker, D. Sept, S. Joseph, M. J. Holst and J. A. McCammon, *Proc Natl Acad Sci U S A*, 2001, 98, 10037-10041.

39. H. Joshi, S. Cheluvaraja, E. Somogyi, D. R. Brown and P. Ortoleva, *Vaccine*, 2011, 29, 9423-9430.

40. H. Joshi, A. Singharoy, Y. V. Sereda, S. C. Cheluvaraja and P. J. Ortoleva, *Progress in biophysics and molecular biology*, 2011, 107, 200-217.

41. J. C. Phillips, R. Braun, W. Wang, J. Gumbart, E. Tajkhorshid, E. Villa, C. Chipot, R. D. Skeel, L. Kale and K. Schulten, *J Comput Chem*, 2005, 26, 1781-1802.

42. A. D. MacKerell, D. Bashford, M. Bellott, R. L. Dunbrack, J. D. Evanseck, M. J. Field, S. Fischer, J. Gao, H. Guo, S. Ha, D. Joseph-McCarthy, L. Kuchnir, K. Kuczera, F. T. Lau, C. Mattos, S. Michnick, T.

Ngo, D. T. Nguyen, B. Prodhom, W. E. Reiher, B. Roux, M. Schlenkrich, J. C. Smith, R. Stote, J.
Straub, M. Watanabe, J. Wiorkiewicz-Kuczera, D. Yin and M. Karplus, *The journal of physical
chemistry. B*, 1998, 102, 3586-3616.

43.   W. Humphrey, A. Dalke and K. Schulten, *Journal of molecular graphics*, 1996, 14, 33-38, 27-38.

44.   J. Schlitter, *Chem Phys Lett*, 1993, 215, 617-621.

45.   N. M. Glykos, *J Comput Chem*, 2006, 27, 1765-1768.

Figure legends

Figure 1.   Crystal structures of the two H5 HA-specific CTL epitopes, RI-10 and
KI-10, in complex with HLA-A*0201. (A) RI-10/KI-10 (H5 HA 198-207), depicted
as red spheres, are located on the upper face of HA and partly overlap with the HA
receptor binding site. (B) Overviews of the crystal structures of RI-10 in complex
with HLA-A*0201 and of KI-10 in complex with HLA-A*0201. (C) Alignment of
RI-10-HLA-A*0201 and KI-10-HLA-A*0201. HLA-A*0201 superimposes clearly in
the two structures. The conformations of the two peptides, RI-10 and KI-10, show
obvious differences.

Figure 2.   CD thermal denaturation profiles for RI-10-HLA-A*0201 and
KI-10-HLA-A*0201. The apparent T_m values are indicated. The y-axis for both data
sets was normalized for illustrative purposes and does not indicate percent completion
of the unfolding transition.

Figure 3.   The structural fluctuation of RI-10- and KI-10-HLA-A*0201 complexes
during MD simulation. (A) RMSF values for each individual residues of the RI-10
and KI-10 peptides. The values represent means ± SE calculated from the last 50 ns of
the three 100 ns simulations on RI-10-HLA-A*0201 and KI-10-HLA-A*0201
complexes. (B) The conformations of KI-10 and RI-10 peptides in the representative
structures of their respective clusters derived from the RMSD-based clustering
analysis. The RMSD cutoff was set to 1.5 Å. (C) RMSF values for individual residues
of the RI-10- and KI-10- bound HLA-A*0201 HC and the differences between them.
The values represent means calculated from the last 50 ns of the three 100 ns
simulations on the two pMHC complexes. **(D)** RMSF values for individual residues of
the   empty   HLA-A*0201   HC   molecules   extracted   from   RI-10-   and
KI-10-HLA-A*0201 complexes, and the differences between them. The values

represent means calculated from the last 50 ns of the three 100 ns simulations on the two empty HLA-A*0201 HC molecules.

Figure 4. Atom contacts between the first residues of RI-10 or KI-10 peptide and HLA-A*0201 HC during MD simulations. (A) The normal distribution of counts of the residues in HLA-A*0201 HC that made atom contacts with Arg1 of RI-10 or Lys1 of KI-10 during the MD simulations. The last 50 ns trajectories of the three 100 ns simulations on RI-10- or KI-10- HLA-A*0201 HC were respectively concatenated into single trajectories for the analysis. (B) Superposition of representative RI-10- and KI-10-HLA-A*0201 complex structures (the structures that were the most similar to the average structures) of the concatenated trajectories of the RI-10- or KI-10-HLA-A*0201 complexes. (C) The residues in HLA-A*0201 HC that made atom contacts with Arg1 of RI-10 in the representative RI-10-HLA-A*0201 complex structure. (D) The residues in HLA-A*0201 HC that made atom contacts with Lys1 of KI-10 in the representative KI-10-HLA-A*0201 complex structure. (E) Salt bridges formed between Arg1 of RI-10 in the representative RI-10-HLA-A*0201 complex structure. (F) Distance between the NH1, NH2 or NE atom of Arg1 in RI-10 and the OE1 or OE2 atom of Glu63 in HLA-A*0201 during one 100 ns simulation on RI-10-HLA-A*0201 complex.

Figure 5. CTL response induced by RI-10/KI-10 in HLA-A*0201/K^b transgenic mice. HLA-A*0201/K^b transgenic mice were immunized with RI-10 or KI-10 emulsified with incomplete Freund's adjuvant (IFA) three times at an interval of 10 days. The mice in the control group were immunized with only IFA. Each group contains four mice. Ten days after the last immunization, splenocytes were isolated and stimulated with RI-10 or KI-10 *in vitro* for 16 hours. CTL response was evaluated by counting IFN-γ-producing cells using ELISPOT assay.
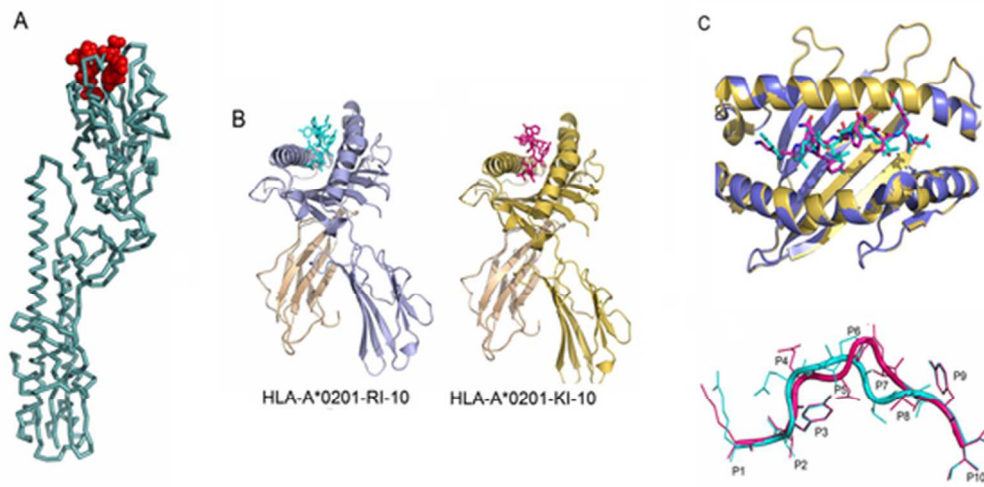
46x24mm (300 x 300 DPI)
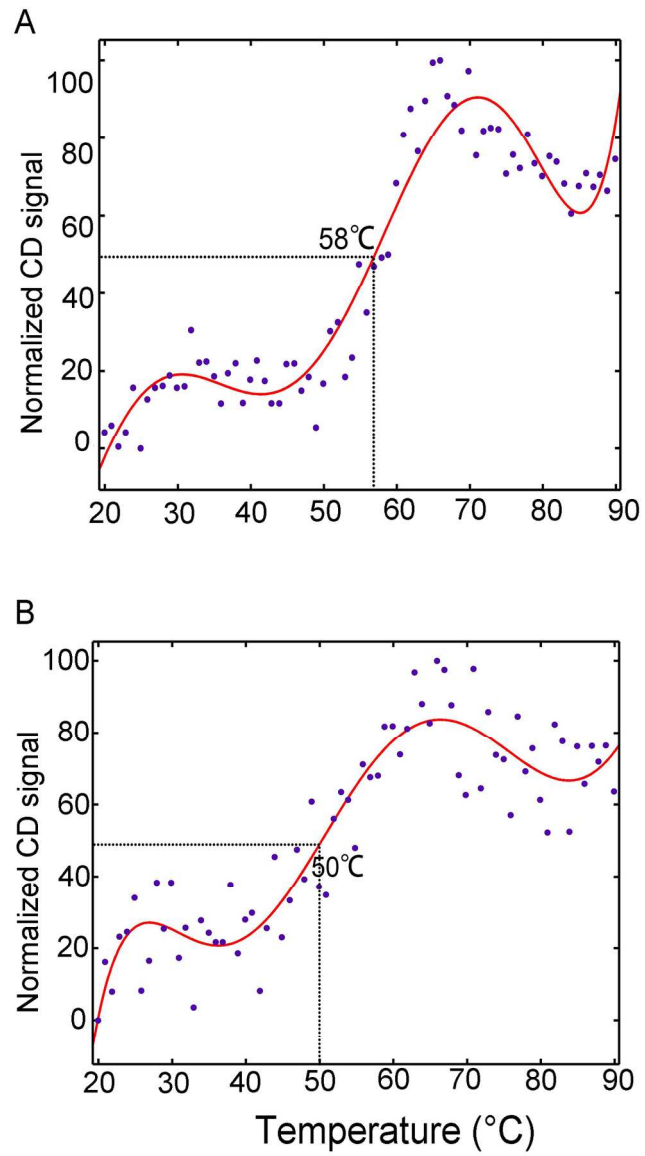
118x206mm (300 x 300 DPI)
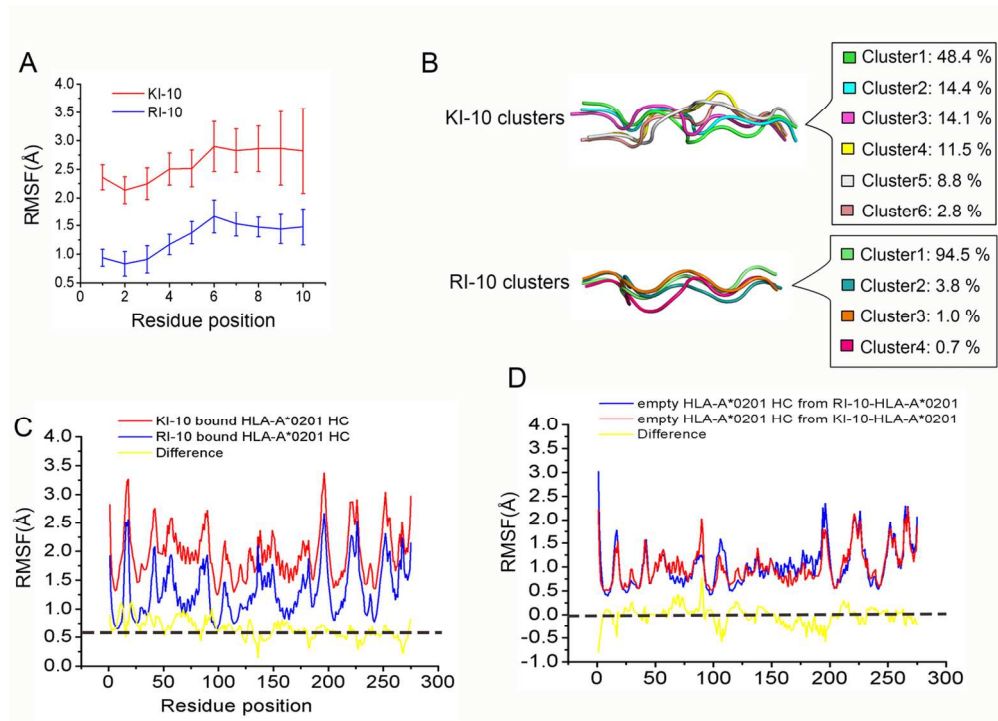
129x93mm (300 x 300 DPI)
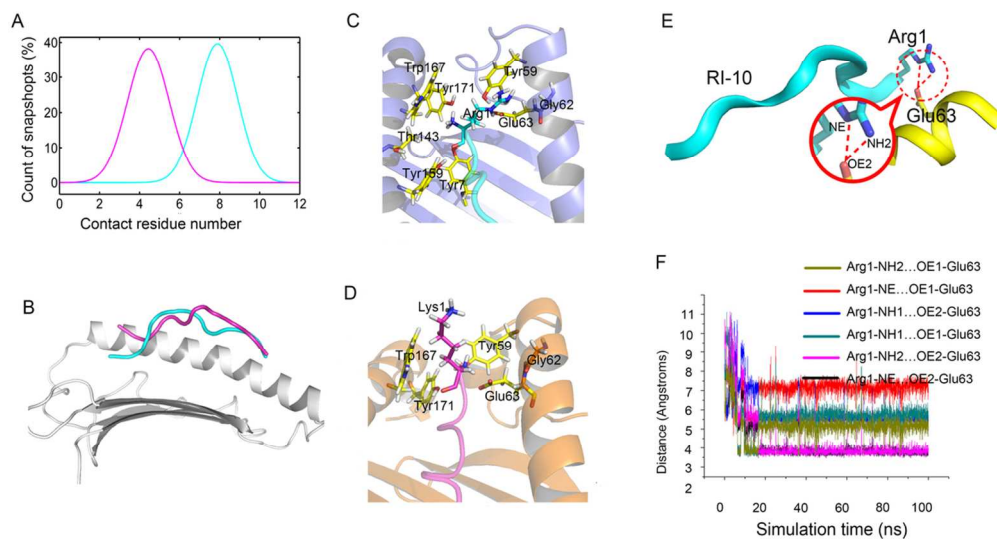
107x61mm (300 x 300 DPI)
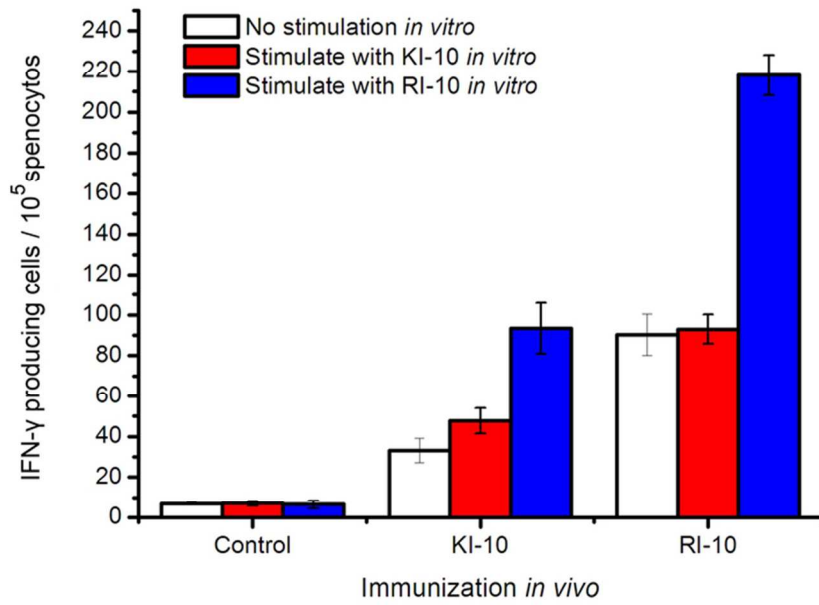
73x47mm (300 x 300 DPI)
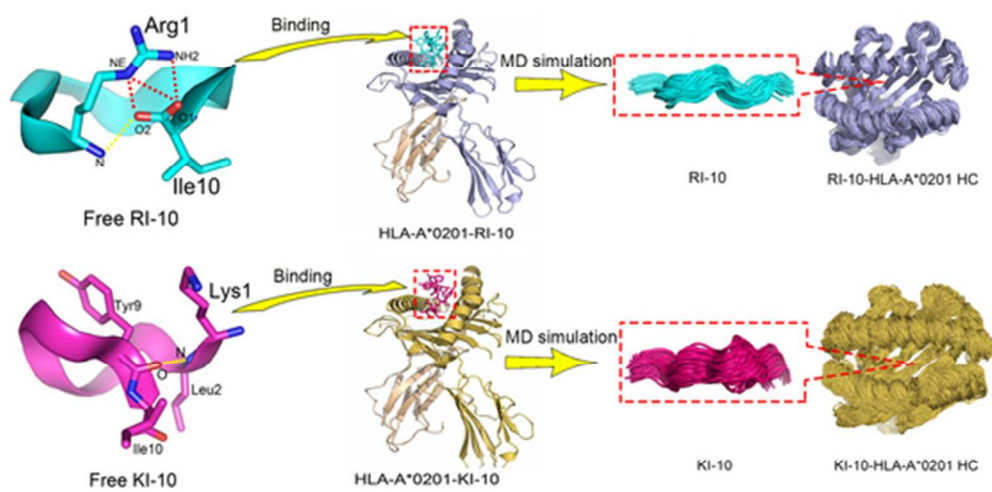
Table of contents entry

The free RI-10 and KI-10 peptides showed bent rather than extended conformations as binding in the cleft of the HLA-A*0201 molecule, and KI-10-HLA-A*0201 processed a much higher flexibility than RI-10-HLA-A*0201.

47x28mm (300 x 300 DPI)